Co-rotating rigid beam with generalized plastic hinges for the nonlinear dynamic analysis of planar framed structures subjected to impact loading

Piseth Heng[a,b], Anas Alhasawi[a], Jean-Marc Battini[b], Mohammed Hjiaj[a,*]

[a] INSA de Rennes, LGCGM/Structural Engineering Research Group, Université Européenne de Bretagne, 20 avenue des Buttes de Coësmes, CS 70839, 35708 Rennes Cedex 7, France
[b] Department of Civil and Architectural Engineering, KTH, Royal Institute of Technology, SE-10044 Stockholm, Sweden

Abstract

The purpose of this paper is to model the nonlinear dynamical response of the steel frame structures subjected to impact loading. A 2D co-rotational rigid beam element with generalized elasto-plastic hinges is presented. The main idea is to integrate the concept of the generalized elasto-plastic hinge into the standard co-rotational framework by performing a static condensation procedure in order to remove the extra internal nodes and their corresponding degrees of freedom. In addition, the impact loading is applied through the contact model that is described in the rigorous framework of the non-smooth dynamics. In this framework, the equations of motion are derived using a set of differential measures and convex analysis tools, whereas Newton's impact law is imposed by means of a restitution coefficient to accommodate energy losses. An energy and momentum conserving scheme is adopted to solve the dynamical equations. The main interest of the current model is the ability to evaluate the geometrically nonlinear inelastic behaviour of the steel structures with semi-rigid connections subjected to impact in a simple and efficient way, using only a few number of elements. The accuracy of the proposed formulation is assessed in three numerical applications.

Keywords : Impact; Non-smooth analysis; Steel Structures; Semi-Rigid Connection; Generalized Elasto-Plastic Hinge; Co-Rotational Element

1. Introduction

Steel frame buildings with semi-rigid connections are common in present-day construction. The service uses of such buildings might expose them to extreme loading conditions such as impact and

*Corresponding author.
Email address: mohammed.hjiaj@insa-rennes.fr (Mohammed Hjiaj)

explosion, which may cause the structures to undergo large displacement and inelastic deformation. In previous decades, the inelastic behaviour of the structures has been statically [1, 2, 3, 4] and dynamically [5, 6, 7] studied using finite element models with a distributed plasticity approach. Although this distributed plasticity approach can accurately capture the inelastic behaviour of the structures, it is inconvenient for practical usage. It requires a large number of stress-strain sampling points through the cross-section and along the member length in order to accurately consider the plastic effects. As an alternative, the lumped plasticity approach requires fewer discrete elements, but the solution is less accurate since the plasticity is lumped at the ends of the element by means of zero-length plastic hinges. Enjoying the simplicity benefit of the lumped plasticity approach, the plastic hinge concept has been adopted in various settings with different levels of enhancements [8, 9, 10, 11, 12]. For instance, Attalla et al [8] developed an element formulation with a non-zero quasi-plastic hinge. Their formulation is able to account for gradual plastification of the cross-section under combined bending and axial forces based on fitting the nonlinear equations to the data obtained from the inelastic and numerical integration of the cross section model along the member length. Liew et al [11] introduced a refined plastic hinge formulation that accounts for the degradation of the element stiffness in the process where the second-order forces at critical locations in the element reach the cross-section plastic strength. On the other hand, we proposed in [12] a simplified formulation with generalised elasto-plastic hinges, which assumes both elasticity and plasticity at the hinges while the element remains rigid at all time. It is worth to point out that sophisticated hinge approaches as described above could have been considered. However, since the purpose of this paper is to propose a model for impact analysis where simplicity and effectiveness are the most visible characteristics of the model, it was decided to not adopt complex approaches and to retain the generalized elasto-plastic hinge model which is briefly described in Section 2.2. The plasticity is consistently accounted for by using non-zero length generalised elasto-plastic hinges, and the second order effect in plasticity is considered by the M-N interaction with superelliptic yield surfaces.

The co-rotational method has been widely used to derive the formulation of the highly nonlinear beam elements for its ability to combine accuracy with numerical efficiency [1, 2, 13, 14, 15, 16]. The underlying concept of the co-rotational formulation is the decomposition of the motion of the element into rigid body part and pure deformational counterpart through the use of a reference system that rotates and translates along with the element. Previously, there have been some efforts devoted to applying the lumped plasticity approach to the co-rotational formulation [18, 19]. However, only static response is investigated, or indeed, only a zero-length plastic hinge that does not accurately capture the plasticity through the proper M-N interaction. Alhasawi et al in [20], for the first time, developped a super-element that consists of a flexible elastic beam with generalized elasto-plastic hinges in the co-rotational framework for a static and cyclic behaviour of frame structures.

In this paper, we present a co-rotational element model for the nonlinear dynamic analysis of steel frame structures subjected to impact. The model includes the inelasticity of the structures by adopting the generalised elasto-plastic hinge concept that is integrated into the co-rotational framework. Hence, the co-rotational element is developed by introducing generalised elasto-plastic hinges at both ends of the rigid element. These hinges induce additional degrees of freedom that are eliminated by static condensation. The behaviour of the generalized hinges is governed by a superelliptic yield criterion, whose shape is controlled by the shape parameters. This type of yield criterion can be used to reproduce the behaviour of joints, as will be shown in one numerical example. It should be informed that this model is an extension of the model developped in [20] in order to have a simpler model and with an application to a dynamical analysis of frame structures subjected to impact.

For the impact, the contact model is developed in a sound and rigorous framework of non-smooth dynamics, in which the equations of motion are derived using a set of differential measures and convex analysis tools. Velocity jumps at impact instants are considered using Newton's impact law by means of restitution coefficient to account for possible energy losses during the collisions. A consistent energy and momentum conserving scheme inherited from the method developed by Chhang et al in [17] is employed to solve the equations of motion.

The outline of the paper is as follows. In section 2, the co-rotational kinematics and the formulation of the elasto-plastic hinges are described. The local element formulation is then given in detail in Section 3. Section 4 provides the dynamical equations derived from the Hamilton's principle and the energy conserving time integration scheme. The impact loading is addressed in Section 5 and numerical examples are presented in Section 6. Finally, conclusions are derived in Section 7.

2. Co-rotational rigid beam element with generalized hinges

In the current model, the structural member consists of three subelements: a rigid beam element and two generalized elasto-plastic hinges that are modeled by a combination of axial and rotational springs, as shown in Fig. 1. The generalized elasto-plastic hinges can be viewed as finite elements with zero initial length. Assembling these hinges with the rigid beam element gives a two-node superelement that is regarded as an individual element fitted for computational purposes. The deformation of the superelement is assumed to be concentrated only at the hinges while the beam element remains rigid. In addition, the generalized hinges are able to rotate and to stretch according to the elasto-plastic constitutive relationships expressed in the incremental form. The yield criterion of the elasto-plastic hinges governs the plastic flow, i.e. the plastic rotation and the plastic elongation/shortening, in the stress-resultant space with the normality rule.

2.1. kinematics

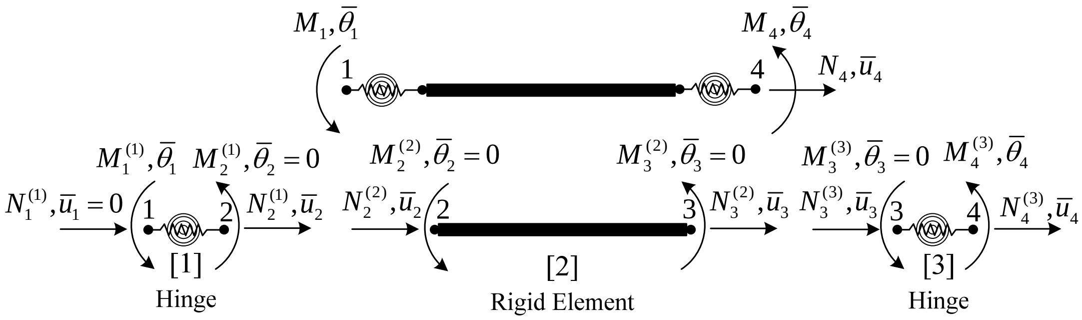

Figure 1: Local superelement

The notations used in this section are defined in Figs. 1 and 2. The origin of the co-rotational frame is taken at node 1 located at the centroid of the cross-section. The x-axis of the local coordinate system is defined by the line connecting node 1 to node 4, see Fig. 2. The y-axis is orthogonal to the x-axis so that the result is right-handedly orthogonal coordinate system. The motion of the superelement from the original undeformed to the actual deformed configuration can thus be separated into two parts. The first part, which corresponds to a rigid motion of the local frame, is the translation of node 1 and the rotation α of the x-axis. The second one refers to the deformations in the co-rotating superelement frame.

The subscript and the superscript denote the node number and the subelement number, respectively. The coordinates of nodes 1 and 4 in the global coordinate system (X, Y) are referred to by (X_1, Y_1) and (X_4, Y_4), respectively. In the deformed configuration (see Fig. 2), the global and local nodal rotations of the superelement (nodes 1 and 4) are notated by θ_1 and θ_4, and $\bar{\theta}_1$ and $\bar{\theta}_4$, respectively.

The total elongation of the superelement $\bar{u}$ is composed of the elongation of the first hinge $\bar{u}_{(12)}$ and the elongation of the second hinge $\bar{u}_{(34)}$, that is

$$\bar{u} = \bar{u}_4 = \bar{u}_{(12)} + \bar{u}_{(34)} \tag{1}$$

with

$$\begin{aligned} \bar{u}_{(12)} &= \bar{u}_2 - \bar{u}_1 \\ \bar{u}_{(34)} &= \bar{u}_4 - \bar{u}_3 \end{aligned} \tag{2}$$

The global and local displacement vectors are respectively defined by:

$$\boldsymbol{q} = \left[\begin{array}{cccccc} u_1 & v_1 & \theta_1 & u_4 & v_4 & \theta_4 \end{array} \right]^{\mathrm{T}} \tag{3}$$

$$\bar{\boldsymbol{q}} = \left[\begin{array}{ccc} \bar{\mathrm{u}} & \bar{\theta}_1 & \bar{\theta}_4 \end{array} \right]^{\mathrm{T}} \tag{4}$$

Referring to the definition of the co-rotating frame (see Fig. 2), the components of the local displacement vector $\bar{\boldsymbol{q}}$ can be calculated as

$$\bar{u} = l - l_0 \tag{5a}$$

$$\bar{\theta}_1 = \theta_1 - \alpha \tag{5b}$$

$$\bar{\theta}_4 = \theta_4 - \alpha \tag{5c}$$

where the initial and final length of the element respectively, defined as l_0 and l, are obtained by

$$l_0 = \sqrt{(X_4 - X_1)^2 + (Y_4 - Y_1)^2} \tag{6a}$$

$$l = \sqrt{(X_4 + u_4 - X_1 - u_1)^2 + (Y_4 + v_4 - Y_1 - v_1)^2} \tag{6b}$$

With the help of basic geometric considerations, the rigid rotation of the x-axis α, featured in Eqs. (5b) and (5c), is computed as

$$\sin\alpha = c_0\, s - s_0\, c \tag{7a}$$

$$\cos\alpha = c_0\, c + s_0\, s \tag{7b}$$

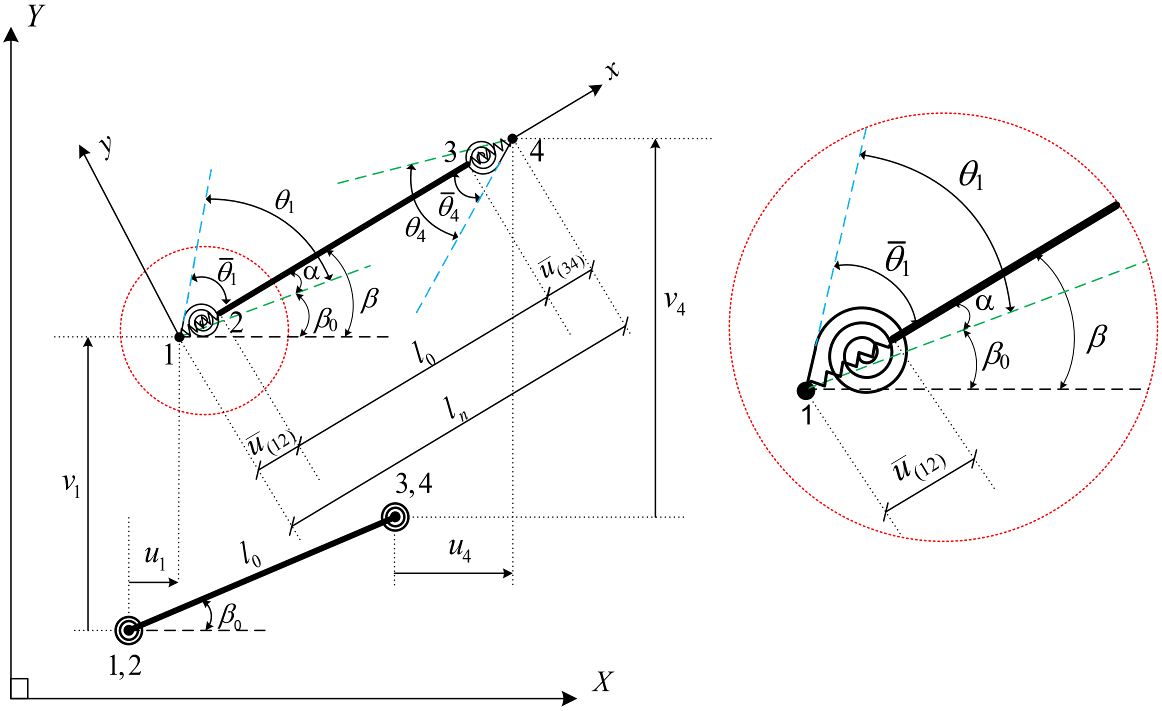

Figure 2: Superelement kinematic 1

with

$$c = \cos\beta = \frac{1}{l}(X_4 + u_4 - X_1 - u_1) \tag{8a}$$

$$c_0 = \cos\beta_0 = \frac{1}{l_0}(X_4 - X_1) \tag{8b}$$

$$s = \sin\beta = \frac{1}{l}(Y_4 + v_4 - Y_1 - v_1) \tag{8c}$$

$$s_0 = \sin\beta_0 = \frac{1}{l_0}(Y_4 - Y_1) \tag{8d}$$

The relationship between the local and global displacements are obtained by the differentiation of Eqs. (5). This gives

$$\delta\bar{\boldsymbol{q}} = \boldsymbol{B}\,\delta\boldsymbol{q} \tag{9}$$

where the transformation matrix, $\boldsymbol{B}$, is given by

$$\boldsymbol{B} = \begin{bmatrix} -c & -s & 0 & c & s & 0 \\ -\frac{s}{l} & \frac{c}{l} & 1 & \frac{s}{l} & -\frac{c}{l} & 0 \\ -\frac{s}{l} & \frac{c}{l} & 0 & \frac{s}{l} & -\frac{c}{l} & 1 \end{bmatrix} \tag{10}$$

2.2. Generalized elasto-plastic hinges

The present model assumes that both elasticity and plasticity are lumped into axial and rotational springs located at the ends of the rigid bar. The elastic stiffness of the hinge is determined considering the energy equivalency between the rigid beam with hinges and the actual clamped-clamped beam member. The elastic behavior of a generalized hinge is uncoupled whereas axial-moment interaction is considered in the plastic range. We adopt the total generalized strain rate decomposition into elastic and plastic parts

$$\dot{\boldsymbol{\Xi}} = \dot{\boldsymbol{\Xi}}^e + \dot{\boldsymbol{\Xi}}^p \tag{11}$$

where $\dot{\boldsymbol{\Xi}} = \left[\dot{\bar{u}}, \dot{\bar{\theta}}\right]^{\mathrm{T}}$. For an associated flow rule, the direction of the generalized plastic strain rate vector is given by the gradient to the yield function, with its magnitude given by the plastic multiplier rate $\dot{\mu}$:

$$\dot{\boldsymbol{\Xi}}^p = \dot{\mu}\,\frac{\partial \Phi}{\partial \boldsymbol{\Sigma}} \tag{12}$$

where $\boldsymbol{\Sigma} = [\,N, M\,]^{\mathrm{T}}$ is the generalized stress vector containing the bending and axial forces in the hinge. The plastic multiplier $\dot{\mu}$ is determined by the classical complementary conditions:

$$\dot{\mu} \geq 0, \qquad \Phi(N, M) \leq 0, \qquad \dot{\mu}\Phi(N, M) = 0 \tag{13}$$

Assuming linear elastic behaviour, the generalized stresses are given as:

$$\boldsymbol{\Sigma} = \mathbb{C}_e\left(\boldsymbol{\Xi} - \boldsymbol{\Xi}^p\right) \tag{14}$$

in which the elastic stiffness matrix is given by:

$$\mathbb{C}_e = \begin{bmatrix} k_{\bar{u}} & 0 \\ 0 & k_{\bar{\theta}} \end{bmatrix}$$

For the hinge that forms at the cross-section of the member, the initial axial and rotational stiffness are $k_{\bar{u}} = 2\dfrac{EA}{L}$ and $k_{\bar{\theta}} = 6\dfrac{EI}{L}$, respectively. E, I, L and A denote the Young modulus, the second moment of the cross-section, the length of the element and the area of the cross-section. In this paper, we adopt a family of the generalized superelliptic yield shapes , which is governed by

$$\Phi(M, N) = \left(\left|\frac{M}{M^p}\right|^{\alpha} + \left|\frac{N}{N^p}\right|^{\beta}\right)^{\frac{1}{\gamma}} - 1 \tag{15}$$

where α, β and γ are the parameters that control the yield shape. For example, the case of $\alpha = 1$, $\beta = 2$ and $\gamma = 1$ corresponds to the yield shape of a rectangular cross-section. The readers are referred to [12] for the detail of the discrete time integration of the equation of the elasto-plastic hinges.

3. Local element formulation

This section will be devoted to the elaboration of the local stiffness matrix. Illustrated by Fig. 1, the superelement is composed of three sub-elements: a rigid beam element and two generalized elasto-plastic hinges. The introduction of the generalised hinges at the rigid beam element's ends increases the number of degrees of freedom exceeding the original ones in the standard co-rotational formulation. By the definition of the co-rotational framework, the displacement of node 1 is zero ($\bar{u}_1 = 0$) in the local coordinate. The elongation/shortening or relative axial displacement of each hinge are denoted by $\bar{u}_{(ij)} = \bar{u}_j - \bar{u}_i$ (Eqs. (2)).

The subelement 1, i.e. an elasto-plastic hinge, has an axial elongation $\bar{u}_{(12)}$ and a rotation $\bar{\theta}_{(12)} = \bar{\theta}_2 - \bar{\theta}_1$. Because the beam element is rigid, its local rotation at node 2 and 3 are zero ($\bar{\theta}_2 = 0$, $\bar{\theta}_3 = 0$). The incremental relation between the stress-resultants and their conjugates can be formally written as

$$\left\{ \begin{array}{c} \Delta N_2^{(1)} \\ \Delta M_2^{(1)} \end{array} \right\} = \begin{bmatrix} C_{11}^{(1)} & C_{12}^{(1)} \\ C_{21}^{(1)} & C_{22}^{(1)} \end{bmatrix} \left\{ \begin{array}{c} \Delta \bar{u}_{(12)} \\ \Delta \bar{\theta}_{(12)} \end{array} \right\} = \begin{bmatrix} C_{11}^{(1)} & -C_{12}^{(1)} \\ C_{21}^{(1)} & -C_{22}^{(1)} \end{bmatrix} \left\{ \begin{array}{c} \Delta \bar{u}_2 \\ \Delta \bar{\theta}_1 \end{array} \right\} \tag{16}$$

where the tangent operator matrix $\mathbb{C}$ is defined by

$$\mathbb{C}_{n+\frac{1}{2}} = \begin{bmatrix} C_{11} & C_{12} \\ C_{21} & C_{22} \end{bmatrix} \tag{17}$$

The reader is referred to [12] for detailed information on how to compute this tangent matrix for various shapes of the yield criterion of the elasto-plastic hinges.

In addition, the incremental equilibrium of the first subelement imposes that

$$\Delta M_1^{(1)} + \Delta M_2^{(1)} = 0 \tag{18}$$

Combining Eqs. (16) and (18) gives

$$\left\{ \begin{array}{c} \Delta M_1^{(1)} \\ \Delta N_2^{(1)} \end{array} \right\} = \begin{bmatrix} C_{22}^{(1)} & -C_{21}^{(1)} \\ -C_{12}^{(1)} & C_{11}^{(1)} \end{bmatrix} \left\{ \begin{array}{c} \Delta \bar{\theta}_1 \\ \Delta \bar{u}_2 \end{array} \right\} \tag{19}$$

On the other hand, the subelement 3, which is also an elasto-plastic hinge, has an axial elongation $\bar{u}_{(34)}$ and a rotation $\bar{\theta}_{(34)} = \bar{\theta}_3 - \bar{\theta}_4$. For this subelement, the incremental relation between the stress-resultants and their conjugates can be formally written as

$$\begin{Bmatrix} \Delta N_4^{(3)} \\ \Delta M_4^{(3)} \end{Bmatrix} = \begin{bmatrix} C_{11}^{(3)} & C_{12}^{(3)} \\ C_{21}^{(3)} & C_{22}^{(3)} \end{bmatrix} \begin{Bmatrix} \Delta \bar{u}_{(34)} \\ \Delta \bar{\theta}_{(34)} \end{Bmatrix} = \begin{bmatrix} C_{11}^{(3)} & C_{12}^{(3)} \\ C_{21}^{(3)} & C_{22}^{(3)} \end{bmatrix} \begin{Bmatrix} \bar{u}_4 - \bar{u}_3 \\ \Delta \bar{\theta}_4 \end{Bmatrix} \tag{20}$$

Furthermore, the incremental equilibrium of subelement 3 requires that

$$\Delta N_3^{(3)} + \Delta N_4^{(3)} = 0 \tag{21}$$

Combining Eqs. (20) and (21) obtains

$$\begin{Bmatrix} \Delta N_3^{(3)} \\ \Delta N_4^{(3)} \\ \Delta M_4^{(3)} \end{Bmatrix} = \begin{bmatrix} C_{11}^{(3)} & -C_{11}^{(3)} & -C_{12}^{(3)} \\ -C_{11}^{(3)} & C_{11}^{(3)} & C_{12}^{(3)} \\ -C_{21}^{(3)} & C_{21}^{(3)} & C_{22}^{(3)} \end{bmatrix} \begin{Bmatrix} \Delta \bar{u}_3 \\ \Delta \bar{u}_4 \\ \Delta \bar{\theta}_4 \end{Bmatrix} \tag{22}$$

Last, the subelement 2 is a rigid element. Since the rigid element does not bend or elongate, writing the bending equilibrium equations of nodes 2 and 3 as well as of the rigid element is unnecessary. The axial equilibrium is, however, important for the condensation process. Based on Fig. 1, the axial equilibrium can be written as

$$\Delta N_2^{(1)} + \Delta N_3^{(3)} = 0 \tag{23}$$

The local displacements of all the points on the rigid beam element are the same. This provides

$$\bar{u}_3 = \bar{u}_2 \tag{24}$$

The above equilibrium equations (Eqs. (19) and (22)) pertain to the end nodes (nodes 1 and 4) at the superelement level by

$$\begin{aligned} \Delta M_1 &= \Delta M_1^{(1)} \\ \Delta N_4 &= \Delta N_4^{(3)} \\ \Delta M_4 &= \Delta M_4^{(3)} \end{aligned} \tag{25}$$

The assembling of the three subelements is accomplished by combining Eqs. (19), (22), (23), and (24). Introducing Eqs. (25) to the outcome gives

$$\begin{Bmatrix} \Delta M_1 \\ 0 \\ \Delta N_4 \\ \Delta M_4 \end{Bmatrix} = \begin{bmatrix} C_{22}^{(1)} & -C_{21}^{(1)} & 0 & 0 \\ -C_{12}^{(1)} & C_{11}^{(1)} + C_{11}^{(3)} & -C_{11}^{(3)} & -C_{12}^{(3)} \\ 0 & -C_{11}^{(3)} & C_{11}^{(3)} & C_{12}^{(3)} \\ 0 & -C_{21}^{(3)} & C_{21}^{(3)} & C_{22}^{(3)} \end{bmatrix} \begin{Bmatrix} \Delta \bar{\theta}_1 \\ \Delta \bar{u}_2 \\ \Delta \bar{u}_4 \\ \Delta \bar{\theta}_4 \end{Bmatrix} \tag{26}$$

The local internal force vector $\boldsymbol{f}_l$ associated with the local displacement vector $\bar{\boldsymbol{q}}$ (Eq. 4) is defined as

$$\boldsymbol{f}_l = \left\{ \begin{array}{ccc} N_4 & M_1 & M_4 \end{array} \right\}^{\mathrm{T}} \tag{27}$$

By using the static condensation of Eq. (26), the local tangent stiffness matrix $\boldsymbol{k}_l$ defined by

$$\Delta \boldsymbol{f}_l = [\boldsymbol{k}_l] \; \Delta \bar{\boldsymbol{q}} \tag{28}$$

and the local displacement $\Delta \bar{u}_2$ can be easily obtained, respectively as

$$k_{l,11} = \frac{C_{11}^{(1)} C_{11}^{(3)}}{C_{11}^{(1)} + C_{11}^{(3)}} \quad ; \quad k_{l,12} = k_{l,21} = -\frac{C_{11}^{(3)} C_{12}^{(1)}}{C_{11}^{(1)} + C_{11}^{(3)}} \tag{29}$$

$$k_{l,13} = k_{l,31} = \frac{C_{11}^{(1)} C_{12}^{(3)}}{C_{11}^{(1)} + C_{11}^{(3)}} \quad ; \quad k_{l,23} = k_{l,32} = -\frac{C_{12}^{(1)} C_{12}^{(3)}}{C_{11}^{(1)} + C_{11}^{(3)}} \tag{30}$$

$$k_{l,22} = C_{22}^{(1)} - \frac{\left(C_{12}^{(1)}\right)^2}{C_{11}^{(1)} + C_{11}^{(3)}} \quad ; \quad k_{l,33} = C_{22}^{(3)} - \frac{\left(C_{12}^{(3)}\right)^2}{C_{11}^{(1)} + C_{11}^{(3)}} \tag{31}$$

and

$$\Delta \bar{u}_2 = \frac{C_{11}^{(3)} \, \bar{u} + C_{12}^{(1)} \, \bar{\theta}_1 + C_{12}^{(3)} \, \bar{\theta}_4}{C_{11}^{(1)} + C_{11}^{(3)}} \tag{32}$$

4. Dynamic equations and time integration scheme

An energy momentum integration scheme based on the midpoint rule is combined to the co-rotational framework in order to derive the dynamic equations. One interesting feature of this approach, see [17], is that the total energy of the system is conserved for elastic problems and that the linear and angular momenta remain constants in absence of external load. Another interesting aspect in the present context is that the contact equations can be introduced in the scheme in a rather simple way.

4.1. Hamilton's principle

Hamilton's principle states that the integral of the Lagrangian between two specified time instances t_1 and t_2 of a conservative mechanical system is stationary:

$$\delta \int_{t_1}^{t_2} \mathcal{L} \, dt = \int_{t_1}^{t_2} \left(\delta \mathcal{K} - \delta \mathcal{U}_{int} - \delta \mathcal{U}_{ext} \right) \, dt = 0 \tag{33}$$

where $\mathcal{K}$, $\mathcal{U}_{int}$ and $\mathcal{U}_{ext}$ denote the kinetic energy, the internal and the external potentials, respectively. The total kinetic energy is the sum of the translational and rotational kinetic energies:

$$\delta\mathcal{K} = \int_{l_0} \rho A\, \dot{u}_G\, \delta\dot{u}_G dx + \int_{l_0} \rho A\, \dot{v}_G\, \delta\dot{v}_G dx + \int_{l_0} \rho I\, \dot{\theta}_G\, \delta\dot{\theta}_G dx \tag{34}$$

A is the area of the cross-section, ρ is the density of the material. Since the subelement between the hinges is considered rigid, the displacements (u_G, v_G) and rotation θ_G of the cross-section centroid G are given by

$$u_G = \left(1 - \frac{x}{l_0}\right) u_1 + \frac{x}{l_0}\, u_4 \tag{35}$$

$$v_G = \left(1 - \frac{x}{l_0}\right) v_1 + \frac{x}{l_0}\, v_4 \tag{36}$$

$$\theta_G = \alpha \tag{37}$$

In addition, the internal potential is defined in the local coordinate system by

$$\delta\mathcal{U}_{int} = N_4\, \delta\bar{u}_4 + M_1\, \delta\bar{\theta}_1 + M_4\, \delta\bar{\theta}_4 = \delta\bar{\boldsymbol{q}}^{\mathrm{T}}\, \boldsymbol{f}_l \tag{38}$$

whereas the external potential has the following form:

$$\delta\mathcal{U}_{ext} = -\delta\boldsymbol{q}^{\mathrm{T}}\, \boldsymbol{P} \tag{39}$$

$\boldsymbol{P}$ is the external force vector of concentrated forces and moments at the nodes. Combining Eqs. (34), (38) and (39) with Eq. (33) and using integral by part, the expression of Hamilton's principle can be reformulated as:

$$\begin{aligned} \int_{t_1}^{t_2} \left(\int_{l_0} \rho A\, \ddot{u}_G \delta\dot{u}_G \, \mathrm{d}x + \int_{l_0} \rho A\, \ddot{v}_G \delta\dot{v}_G \, \mathrm{d}x + \int_{l_0} \rho I\, \ddot{\theta}_G \delta\dot{\theta}_G \, \mathrm{d}x \right) \mathrm{d}t + \int_{t_1}^{t_2} \delta\bar{\boldsymbol{q}}^{\mathrm{T}}\, \boldsymbol{f}_l \, \mathrm{d}t \\ - \int_{t_1}^{t_2} \delta\boldsymbol{q}^{\mathrm{T}}\, \boldsymbol{P} \mathrm{d}t = 0 \end{aligned} \tag{40}$$

4.2. Dynamic equations

In the present context of the co-rotational formulation, the midpoint time integration scheme is defined by:

$$\begin{aligned} &\int_{t_1}^{t_2} \boldsymbol{q}\,(t)\, \mathrm{d}t = \boldsymbol{q}\left(t_{n+\frac{1}{2}}\right) \Delta t = \boldsymbol{q}_{n+\frac{1}{2}} \Delta t \\ &\boldsymbol{q}_{n+\frac{1}{2}} = \frac{\boldsymbol{q}_{n+1} + \boldsymbol{q}_n}{2} = \boldsymbol{q}_n + \frac{1}{2}\Delta\boldsymbol{q} \\ &\dot{\boldsymbol{q}}_{n+\frac{1}{2}} = \frac{\dot{\boldsymbol{q}}_{n+1} + \dot{\boldsymbol{q}}_n}{2} = \frac{\boldsymbol{q}_{n+1} - \boldsymbol{q}_n}{\Delta t} = \frac{\Delta\boldsymbol{q}}{\Delta t} \\ &\ddot{\boldsymbol{q}}_{n+\frac{1}{2}} = \frac{\ddot{\boldsymbol{q}}_{n+1} + \ddot{\boldsymbol{q}}_n}{2} = \frac{\dot{\boldsymbol{q}}_{n+1} - \dot{\boldsymbol{q}}_n}{\Delta t} = \frac{2}{\Delta t^2}\Delta\boldsymbol{q} - \frac{2}{\Delta t}\dot{\boldsymbol{q}}_n \end{aligned} \tag{41}$$

Applying Eqs. (41) to Hamilton's principle Eq. (40) gives

$$\delta\boldsymbol{q}^{\mathtt{T}}\left[\int_{l_0}\rho A\,\ddot{u}_{G,n+\frac{1}{2}}\left(\frac{\partial u_{G,n+\frac{1}{2}}}{\partial\boldsymbol{q}_{n+\frac{1}{2}}}\right)^{\mathtt{T}}\mathrm{d}x+\int_{l_0}\rho A\,\ddot{v}_{G}\left(\frac{\partial v_{G,n+\frac{1}{2}}}{\partial\boldsymbol{q}_{n+\frac{1}{2}}}\right)^{\mathtt{T}}\mathrm{d}x\right.$$
$$\left.+\int_{l_0}\rho I\,\ddot{\theta}_{G,n+\frac{1}{2}}\left(\frac{\partial\theta_{G,n+\frac{1}{2}}}{\partial\boldsymbol{q}_{n+\frac{1}{2}}}\right)^{\mathtt{T}}\mathrm{d}x+\left(\frac{\partial\bar{\boldsymbol{q}}_{n+\frac{1}{2}}}{\partial\boldsymbol{q}_{n+\frac{1}{2}}}\right)^{\mathtt{T}}\boldsymbol{f}_{l,n+\frac{1}{2}}-\boldsymbol{P}_{n+\frac{1}{2}}\right]=0 \tag{42}$$

In Eq. (42), the variation $\delta\boldsymbol{q}$ is arbitrary. The global displacements ($\dot{u}_{G,n}$ and $\dot{u}_{G,n}$) at time t_n are related to $\dot{\boldsymbol{q}}_n$ at time t_n from Eqs. (35) and (36) as

$$\dot{u}_{G,n}=\boldsymbol{f}_1^{\mathrm{T}}\,\dot{\boldsymbol{q}}_n \tag{43}$$
$$\dot{v}_{G,n}=\boldsymbol{f}_2^{\mathrm{T}}\,\dot{\boldsymbol{q}}_n \tag{44}$$

By using Eqs. (8c) and (37), the global rotation $\dot{\theta}_{G,n}$ is updated by

$$\dot{\theta}_{G,n+1}=2\,\dot{\theta}_{G,n+\frac{1}{2}}-\dot{\theta}_{G,n}=2\,\boldsymbol{f}_{3,n+\frac{1}{2}}^{\mathrm{T}}\,\frac{\Delta\boldsymbol{q}}{\Delta t}-\dot{\theta}_{G,n} \tag{45}$$

with

$$\boldsymbol{f}_1=\begin{bmatrix}1-\dfrac{x}{l_0} & 0 & 0 & \dfrac{x}{l_0} & 0 & 0\end{bmatrix}^{\mathrm{T}} \tag{46}$$
$$\boldsymbol{f}_2=\begin{bmatrix}0 & 1-\dfrac{x}{l_0} & 0 & 0 & \dfrac{x}{l_0} & 0\end{bmatrix}^{\mathrm{T}} \tag{47}$$
$$\boldsymbol{f}_{3,n+\frac{1}{2}}=\frac{\boldsymbol{z}_{n+\frac{1}{2}}}{l_{n+\frac{1}{2}}} \tag{48}$$
$$\boldsymbol{z}_{n+\frac{1}{2}}=\begin{bmatrix}s_{n+\frac{1}{2}} & -c_{n+\frac{1}{2}} & 0 & -s_{n+\frac{1}{2}} & c_{n+\frac{1}{2}} & 0\end{bmatrix}^{\mathrm{T}} \tag{49}$$

With the help of Eqs. (41) and (43)-(45), the accelerations at time $t_{n+\frac{1}{2}}$ are obtained as

$$\ddot{u}_{G,n+\frac{1}{2}}=\frac{2}{\Delta t^2}\,\Delta u_G-\frac{2}{\Delta t}\,\dot{u}_{G,n}=\frac{2}{\Delta t^2}\,\boldsymbol{f}_1^{\mathrm{T}}\,\Delta\boldsymbol{q}-\frac{2}{\Delta t}\,\boldsymbol{f}_1^{\mathrm{T}}\,\dot{\boldsymbol{q}}_n \tag{50}$$
$$\ddot{v}_{G,n+\frac{1}{2}}=\frac{2}{\Delta t^2}\,\Delta v_G-\frac{2}{\Delta t}\,\dot{v}_{G,n}=\frac{2}{\Delta t^2}\,\boldsymbol{f}_2^{\mathrm{T}}\,\Delta\boldsymbol{q}-\frac{2}{\Delta t}\,\boldsymbol{f}_2^{\mathrm{T}}\,\dot{\boldsymbol{q}}_n \tag{51}$$
$$\ddot{\theta}_{G,n+\frac{1}{2}}=\frac{2}{\Delta t^2}\Delta\theta_G-\frac{2}{\Delta t}\dot{\theta}_{G,n}=\frac{2}{\Delta t^2}\boldsymbol{f}_{3,n+\frac{1}{2}}^{\mathrm{T}}\,\Delta\boldsymbol{q}-\frac{2}{\Delta t}\dot{\theta}_{G,n} \tag{52}$$

The equations of the motion at time $t_{n+\frac{1}{2}}$ are obtained from Eqs. (42) as

$$\boldsymbol{f}_{k,n+\frac{1}{2}}+\boldsymbol{f}_{g,n+\frac{1}{2}}-\boldsymbol{f}_{ext,n+\frac{1}{2}}=0 \tag{53}$$

in which $\boldsymbol{f}_{k,n+\frac{1}{2}}$ is the inertia force vector, $\boldsymbol{f}_{g,n+\frac{1}{2}}$ is the elastic force vector and $\boldsymbol{f}_{ext,n+\frac{1}{2}}$ is the external load vector. The following expression for the inertia force vector $\boldsymbol{f}_{k,n+\frac{1}{2}}$ at midpoint is obtained as:

$$
\begin{aligned}
\boldsymbol{f}_{k,n+\frac{1}{2}} &= \frac{2}{\Delta t^2}\int_{l_0}\left[\rho A\,\left(\boldsymbol{f}_1\boldsymbol{f}_1^{\mathrm{T}}+\boldsymbol{f}_2\boldsymbol{f}_2^{\mathrm{T}}\right)+\rho I\,\boldsymbol{f}_{3,n+\frac{1}{2}}\boldsymbol{f}_{3,n+\frac{1}{2}}^{\mathrm{T}}\right]\Delta\boldsymbol{q}\,\mathrm{d}x \\
&\quad -\frac{2}{\Delta t}\int_{l_0}\left[\rho A\,\left(\boldsymbol{f}_1\boldsymbol{f}_1^{\mathrm{T}}+\boldsymbol{f}_2\boldsymbol{f}_2^{\mathrm{T}}\right)\dot{\boldsymbol{q}}_n+\rho I\,\dot{\theta}_{G,n}\,\boldsymbol{f}_{3,n+\frac{1}{2}}\right]\mathrm{d}x \\
&= \frac{2\,\boldsymbol{m}_q}{\Delta t}\left(\frac{\Delta\boldsymbol{q}}{\Delta t}-\dot{\boldsymbol{q}}_n\right)+\frac{2\rho I\,l_0}{\Delta t}\left(\boldsymbol{f}_{3,n+\frac{1}{2}}\boldsymbol{f}_{3,n+\frac{1}{2}}^{\mathrm{T}}\frac{\Delta\boldsymbol{q}}{\Delta t}-\dot{\theta}_{G,n}\,\boldsymbol{f}_{3,n+\frac{1}{2}}\right)
\end{aligned}
\tag{54}
$$

in which

$$
\boldsymbol{m}_q=\int_{l_0}\rho A\,\left(\boldsymbol{f}_1\boldsymbol{f}_1^{\mathrm{T}}+\boldsymbol{f}_2\boldsymbol{f}_2^{\mathrm{T}}\right)\mathrm{d}x=\rho A\,l_0\begin{bmatrix}\frac{1}{3}&0&0&\frac{1}{6}&0&0\\0&\frac{1}{3}&0&0&\frac{1}{6}&0\\0&0&0&0&0&0\\\frac{1}{6}&0&0&\frac{1}{3}&0&0\\0&\frac{1}{6}&0&0&\frac{1}{3}&0\\0&0&0&0&0&0\end{bmatrix}
\tag{55}
$$

The internal force vector takes the form of

$$
\boldsymbol{f}_{g,n+\frac{1}{2}}=\left(\frac{\partial\bar{\boldsymbol{q}}_{n+\frac{1}{2}}}{\partial\boldsymbol{q}_{n+\frac{1}{2}}}\right)^{\mathrm{T}}\boldsymbol{f}_{l,n+\frac{1}{2}}=\boldsymbol{B}_{n+\frac{1}{2}}^{\mathrm{T}}\boldsymbol{f}_{l,n+\frac{1}{2}}
\tag{56}
$$

The components of the deformation vectors at time $t_{n+\frac{1}{2}}$ are obtained by using Eqs. (5), (6b),(8a) and (8c) as

$$
\bar{u}_{n+\frac{1}{2}}=\bar{u}_n+\frac{1}{2}\Delta\bar{u}=\bar{u}_n+\frac{1}{2}\,\boldsymbol{r}_{n+\frac{1}{2}}^{\mathrm{T}}\Delta\boldsymbol{q}
\tag{57}
$$

$$
\bar{\theta}_{1,n+\frac{1}{2}}=\bar{\theta}_{1,n}+\frac{1}{2}\Delta\bar{\theta}_1=\bar{\theta}_{1,n}+\frac{1}{2}\,\boldsymbol{b}_{1,n+\frac{1}{2}}^{\mathrm{T}}\Delta\boldsymbol{q}
\tag{58}
$$

$$
\bar{\theta}_{4,n+\frac{1}{2}}=\bar{\theta}_{4,n}+\frac{1}{2}\Delta\bar{\theta}_4=\bar{\theta}_{4,n}+\frac{1}{2}\,\boldsymbol{b}_{2,n+\frac{1}{2}}^{\mathrm{T}}\Delta\boldsymbol{q}
\tag{59}
$$

where

$$
\boldsymbol{r}_{n+\frac{1}{2}}=\begin{bmatrix}-c_{n+\frac{1}{2}}&-s_{n+\frac{1}{2}}&0&c_{n+\frac{1}{2}}&s_{n+\frac{1}{2}}&0\end{bmatrix}^{\mathrm{T}}
\tag{60}
$$

$$
\boldsymbol{b}_{1,n+\frac{1}{2}}=\begin{bmatrix}0&0&1&0&0&0\end{bmatrix}^{\mathrm{T}}-\frac{\boldsymbol{z}_{n+\frac{1}{2}}}{l_{n+\frac{1}{2}}}
\tag{61}
$$

$$
\boldsymbol{b}_{2,n+\frac{1}{2}}=\begin{bmatrix}0&0&0&0&0&1\end{bmatrix}^{\mathrm{T}}-\frac{\boldsymbol{z}_{n+\frac{1}{2}}}{l_{n+\frac{1}{2}}}
\tag{62}
$$

Last, the external force vector is defined by

$$\boldsymbol{f}_{ext,n+\frac{1}{2}} = \boldsymbol{P}_{n+\frac{1}{2}} \tag{63}$$

4.3. Tangent matrices

The tangent dynamic and stiffness matrices are obtained through the derivation of Eq. (54) and (56). They are obtained as

$$\begin{aligned}\boldsymbol{K}_{k,n+\frac{1}{2}} = \frac{\partial \boldsymbol{f}_{k,n+\frac{1}{2}}}{\partial\left(\Delta \boldsymbol{q}\right)} = \frac{2\,\boldsymbol{m}_q}{\Delta t^2} + \frac{2\,\rho I l_0}{\Delta t^2}\boldsymbol{f}_{3,n+\frac{1}{2}}\boldsymbol{f}^{\mathrm{T}}_{3,n+\frac{1}{2}} - \frac{1}{2\,l^2_{n+\frac{1}{2}}}\boldsymbol{f}^{\mathrm{T}}_{3,n+\frac{1}{2}}\Delta\boldsymbol{q}\left(\boldsymbol{r}_{n+\frac{1}{2}}\boldsymbol{z}^{\mathrm{T}}_{n+\frac{1}{2}} + \boldsymbol{z}_{n+\frac{1}{2}}\boldsymbol{r}^{\mathrm{T}}_{n+\frac{1}{2}}\right) \\ - \frac{1}{2\,l^2_{n+\frac{1}{2}}}\boldsymbol{f}_{3,n+\frac{1}{2}}\Delta\boldsymbol{q}^{\mathrm{T}}\left(\boldsymbol{r}_{n+\frac{1}{2}}\boldsymbol{z}^{\mathrm{T}}_{n+\frac{1}{2}} + \boldsymbol{z}_{n+\frac{1}{2}}\boldsymbol{r}^{\mathrm{T}}_{n+\frac{1}{2}}\right) + \frac{\rho I l_0\,\dot{\theta}_{G,n}}{\Delta t\, l^2_{n+\frac{1}{2}}}\left(\boldsymbol{r}_{n+\frac{1}{2}}\boldsymbol{z}^{\mathrm{T}}_{n+\frac{1}{2}} + \boldsymbol{z}_{n+\frac{1}{2}}\boldsymbol{r}^{\mathrm{T}}_{n+\frac{1}{2}}\right)\end{aligned} \tag{64}$$

$$\begin{aligned}\boldsymbol{K}_{g,n+\frac{1}{2}} = \frac{\partial \boldsymbol{f}_{g,n+\frac{1}{2}}}{\partial\left(\Delta \boldsymbol{q}\right)} = \frac{1}{2}\boldsymbol{B}^{\mathrm{T}}_{n+\frac{1}{2}}\boldsymbol{k}_{l,n+\frac{1}{2}}\left(\boldsymbol{B}_{n+\frac{1}{2}} + \boldsymbol{B}_{0,n+\frac{1}{2}}\right) + \frac{1}{2}N_{4,n+\frac{1}{2}}\left(\frac{\boldsymbol{z}_{n+\frac{1}{2}}\boldsymbol{z}^{\mathrm{T}}_{n+\frac{1}{2}}}{l_{n+\frac{1}{2}}}\right) \\ + \frac{1}{2}\left(M_{1,n+\frac{1}{2}} + M_{4,n+\frac{1}{2}}\right)\left(\frac{\boldsymbol{r}_{n+\frac{1}{2}}\boldsymbol{z}^{\mathrm{T}}_{n+\frac{1}{2}} + \boldsymbol{z}_{n+\frac{1}{2}}\boldsymbol{r}^{\mathrm{T}}_{n+\frac{1}{2}}}{l^2_{n+\frac{1}{2}}}\right)\end{aligned} \tag{65}$$

where

$$\boldsymbol{B}_{0,n+\frac{1}{2}} = \begin{bmatrix} \Delta\boldsymbol{q}^{\mathrm{T}}\left(\dfrac{\boldsymbol{z}_{n+\frac{1}{2}}\boldsymbol{z}^{\mathrm{T}}_{n+\frac{1}{2}}}{l_{n+\frac{1}{2}}}\right) \\ \Delta\boldsymbol{q}^{\mathrm{T}}\left(\dfrac{\boldsymbol{z}_{n+\frac{1}{2}}\boldsymbol{r}^{\mathrm{T}}_{n+\frac{1}{2}} + \boldsymbol{r}_{n+\frac{1}{2}}\boldsymbol{z}^{\mathrm{T}}_{n+\frac{1}{2}}}{l^2_{n+\frac{1}{2}}}\right) \\ \Delta\boldsymbol{q}^{\mathrm{T}}\left(\dfrac{\boldsymbol{z}_{n+\frac{1}{2}}\boldsymbol{r}^{\mathrm{T}}_{n+\frac{1}{2}} + \boldsymbol{r}_{n+\frac{1}{2}}\boldsymbol{z}^{\mathrm{T}}_{n+\frac{1}{2}}}{l^2_{n+\frac{1}{2}}}\right) \end{bmatrix} \tag{66}$$

4.4. Simplification of the kinetic term

It should be noted that the kinetic expression in Eq. (54) is nonlinear due to the term that corresponds to the rigid rotation, i.e. the second term on the right side of Eq. (54). Since the purpose of this paper is to present a simple model in the co-rotational framework, an alternative option is to neglect the nonlinear term. The influence of this consideration will be illustrated in the numerical examples. In this case, the expression in Eq. (54) becomes

$$\boldsymbol{f}_{k,n+\frac{1}{2}} = \frac{2\,\boldsymbol{m}_q}{\Delta\, t}\left(\frac{\Delta\boldsymbol{q}}{\Delta t} - \dot{q}_n\right) \tag{67}$$

5. Non-smooth dynamic: impact loading

5.1. Contact model

It is assumed in this paper that the structure is impacted at only one of its nodes in a direction denoted by $\boldsymbol{q}(i)$ (Fig. 3). As a result, the model considers the unilateral collision between a rigid point mass m_c and a nodal mass of the structure. The motions of the impacted masses are constrained by the contact conditions, which include the non-penetration and the non-adhesion conditions. These conditions at position level may be summarized by the so-called Signorini's force law:

$$g_N \geq 0 \quad , \quad \lambda_N \geq 0 \quad , \quad g_N \, \lambda_N = 0 \tag{68}$$

where the gap $g_N = \boldsymbol{q}(i) - x_c$. x_c is the position of the mass m_c. λ_N corresponds to the force exerted by the nodal mass on mass m_c: $F_{i \to c}$. According to the principle of action-reaction, the force exerted by mass m_c on the nodal mass ($F_{c \to i}$) is $-\lambda_N$.

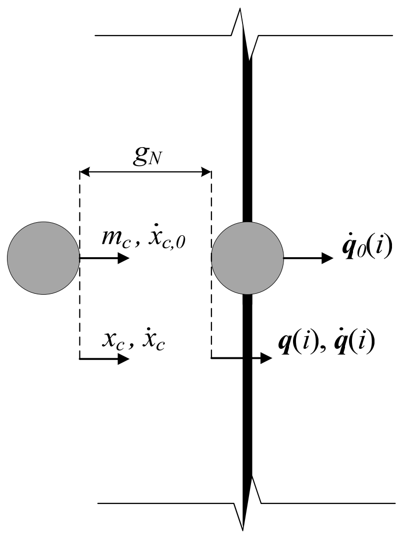

Figure 3: Contact model

The non-smoothness of the impact involves the discontinuity of the velocities; to be physically consistent, the unilateral constraints should be discretized at velocity level and incorporated with Newton's impact law. This combined law is described by

$$\xi_N \geq 0 \quad , \quad -\Lambda_N \leq 0 \quad , \quad \xi_N \Lambda_N = 0 \tag{69}$$

where the relative velocity $\gamma_N = \dot{\boldsymbol{q}}(i) - \dot{x}_c$ and Λ_N is the the percussion force. $\xi_N = \gamma_N^+ + \varepsilon\gamma_N^-$, in which ε denotes the coefficient of restitution. The superscript $(-)$ and $(+)$ are referred to the state before and after impact respectively. The contact model in this paper encounters only one constraint (one impact point). This one constraint problem allows us to determine the contact force directly from the equations of motion combining with the constraint equations, as will be shown in the next section.

5.2. Equation of motion

The motions of the other non-impacted masses are continuous and governed by Eqs. (53). On the other hand, the motions of the impacted masses can be non-smooth and cannot be expressed only by Eqs. (53). It is necessary to write two separate sets of equations depending on the value of the gap g_N if the motion occurs during the closed contact ($g_N = 0$) or during open contact ($g_N > 0$).

For an open contact motion, the contact force disappears, and the motion is smooth. Applying the mid-point rule (Eqs. (41)), the discrete equations of the open-contact motion of the impacted masses are obtained as

$$m_c\,\ddot{x}_{c,n+\frac{1}{2}} = 0 \tag{70}$$

$$\boldsymbol{f}_{k,n+\frac{1}{2}} + \boldsymbol{f}_{g,n+\frac{1}{2}} - \boldsymbol{f}_{ext,n+\frac{1}{2}} = 0 \tag{71}$$

$$g_N > 0 \tag{72}$$

where $\boldsymbol{f}_{k,n+\frac{1}{2}}$, $\boldsymbol{f}_{g,n+\frac{1}{2}}$ and $\boldsymbol{f}_{ext,n+\frac{1}{2}}$ are defined in Eqs. (54), (56) and (63), respectively.

On the other hand, the impact may occur during the closed contact motion and cause the velocity jumps at specific time instants. At those time instances, the velocity of the impacted masses are not differentiable and the contact force is impulsive. The equations of the closed-contact motion are best described by an equality of the differential measures so that the combined equations of motion are obtained to describe both the smooth and the non-smooth parts of the closed contact motion, as suggested by Moreau [21]. By applying the mid-point rule to the differential measure equations and integrating them over time increment $[t_n, t_{n+1}]$, it is obtained

$$m_c\left(\dot{x}_{c,n+1} - \dot{x}_{c,n}\right) = -P_N \tag{73}$$

$$\boldsymbol{m}_q\left(\dot{\boldsymbol{q}}_{n+1} - \dot{\boldsymbol{q}}_n\right) + 2\rho I\, l_0\left(\boldsymbol{f}_{3,n+\frac{1}{2}}\boldsymbol{f}^{\mathrm{T}}_{3,n+\frac{1}{2}}\frac{\Delta\boldsymbol{q}}{\Delta t} - \dot{\theta}_{G,n}\,\boldsymbol{f}_{3,n+\frac{1}{2}}\right) \tag{74}$$

$$+\boldsymbol{f}_{g,n+\frac{1}{2}}\Delta t - \boldsymbol{f}_{ext,n+\frac{1}{2}}\Delta t = P_N\boldsymbol{I}_i$$

$$g_N = 0 \tag{75}$$

$$\xi_N = \gamma_{N,n+1} + \varepsilon\gamma_{N,n} \geq 0 \tag{76}$$

where $\boldsymbol{I}_i$ is a unit vector corresponding to the impacting direction $\boldsymbol{q}(i)$. P_N is the percussion force resulting from the integration of the differential measure of the contact force

$$\int_{t_n}^{t_{n+1}}\left[\lambda_N\,dt + \left(\Lambda^+_N - \Lambda^-_N\right)\,d\eta\right] = P_N \tag{77}$$

In order to solve Eqs. (73)-(76), the following methodology is presented. First, the percussion force P_N is assumed to be zero, and Eqs. (73) and (74) are solved for the displacements of the masses using mid-point scheme (Eqs. (41)). ξ_N is then computed using Eq. (76). If $\xi_N > 0$, the prediction of no percussion force is true. Otherwise, if $\xi_N < 0$, the percussion force P_N exists and has a positive value. In such case, the following equations are solved to calculate the velocities and the displacements of the masses as well as the percussion force:

$$m_c\left(\dot{x}_{c,n+1} - \dot{x}_{c,n}\right) = -P_N \tag{78}$$

$$\boldsymbol{m}_q\left(\dot{\boldsymbol{q}}_{n+1} - \dot{\boldsymbol{q}}_n\right) + 2\rho I\, l_0\left(\boldsymbol{f}_{3,n+\frac{1}{2}}\boldsymbol{f}^{\mathrm{T}}_{3,n+\frac{1}{2}}\frac{\Delta\boldsymbol{q}}{\Delta t} - \dot{\theta}_{G,n}\,\boldsymbol{f}_{3,n+\frac{1}{2}}\right) \tag{79}$$

$$+\boldsymbol{f}_{g,n+\frac{1}{2}}\Delta t - \boldsymbol{f}_{ext,n+\frac{1}{2}}\Delta t = P_N\boldsymbol{I}_i$$

$$\xi_N = \gamma_{N,n+1} + \varepsilon\gamma_{N,n} = 0 \tag{80}$$

6. Numerical examples

In this section, three numerical examples are provided. The purpose of these examples is to assess and validate the dynamic performance of the proposed planar co-rotational rigid beam element with generalized elasto-plastic hinges in modeling the behaviour of the steel frame structure subjected to impact loading. The results are validated against a reference solution obtained by performing a simulation with a commercial finite element program (Abaqus/Explicit v6.14). In these analyses, 2D Timoshenko beam elements (B21) and a default Hilber-Hughes-Taylor time integrator are used. Furthermore, the surface-to-surface contact interaction with a kinematic contact method is adopted for the contact model. In order to ensure the convergence of the reference solution, different mesh densities are tested.

6.1. Example 1

Consider a T-frame structure collided by a rigid point mass $m_c = 1500\,\mathrm{kg}$ with an initial velocity of $v_{c,0} = 50\,\mathrm{m/s}$. The dimension of the structure, the position of the impact, and the cross-section of the members are illustrated in Fig. 4. For all the members in the structure, the following parameters are considered:

- The cross-section depth and width: $a = e = 0.2\,\mathrm{m}$
- The elastic modulus: $E = 210\,\mathrm{GPa}$
- The mass per unit volume: $\rho = 7850\,\mathrm{kg/m^3}$
- The elastic limit: $\sigma_y = 355\,\mathrm{MPa}$

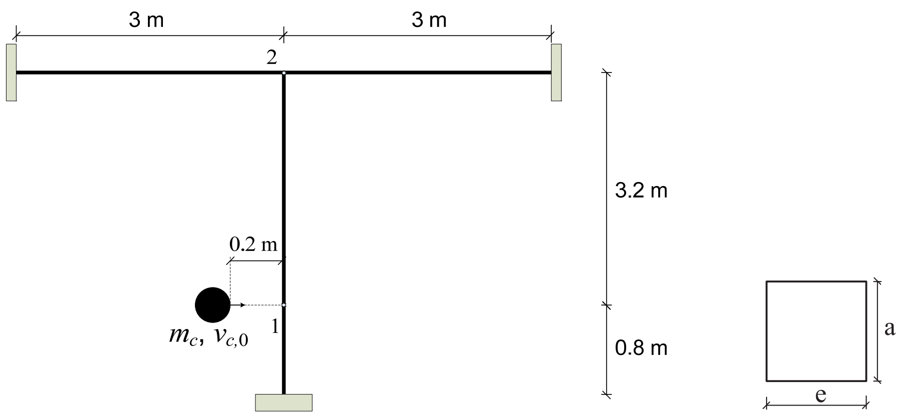

(a) (b)

Figure 4: Example 1: (a) geometry. (b) cross-section.

In the new rigid element formulation, 4 elements are used: one element for one member except the impacted column that requires two elements. The time step size $\Delta t = 10^{-4}\,\mathrm{s}$ and the coefficient of restitution $\varepsilon = 0$ are chosen. On the other hand, the FE simulation requires 200 elements (the size of the element equals 50 mm) in order to have a converged solution.

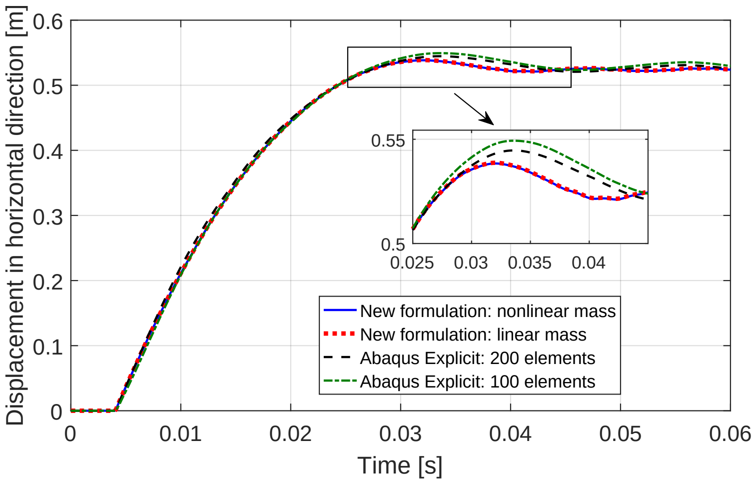

(a) Point 1

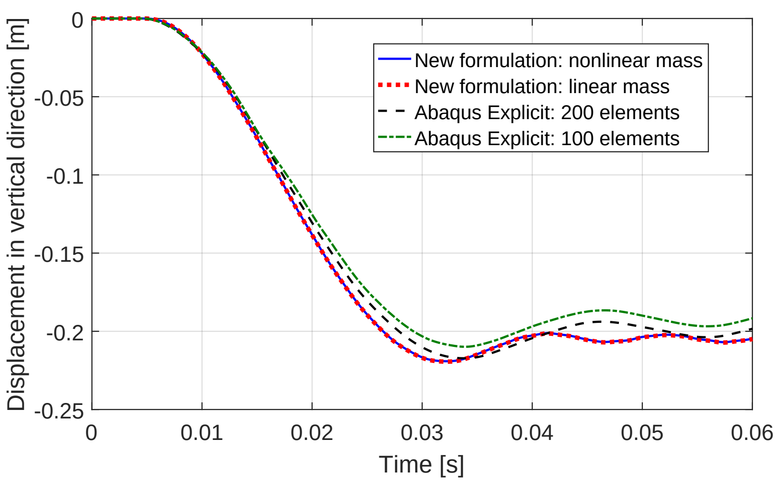

(b) Point 2

Figure 5: Example 1: Evolution of displacement

Fig. 5(a) and 5(b) show the evolution of the displacement of point 1 in horizontal direction and of point 2 in vertical direction, respectively. It can be observed from Fig. 5(a) and 5(b) that the proposed formulation gives results that agree remarkably well with reference solution. From Fig. 5(a), the difference in the maximum displacement of point 1 in horizontal direction between the proposed formulation and the reference FE simulation is about 1 percent. From Fig. 5(b), the difference in the maximum displacement of point 2 in vertical direction between the proposed formulation and the reference FE simulation is approximately 1 percent. Besides, it can be noted that the same results are obtained with the linear and nonlinear inertial expressions.

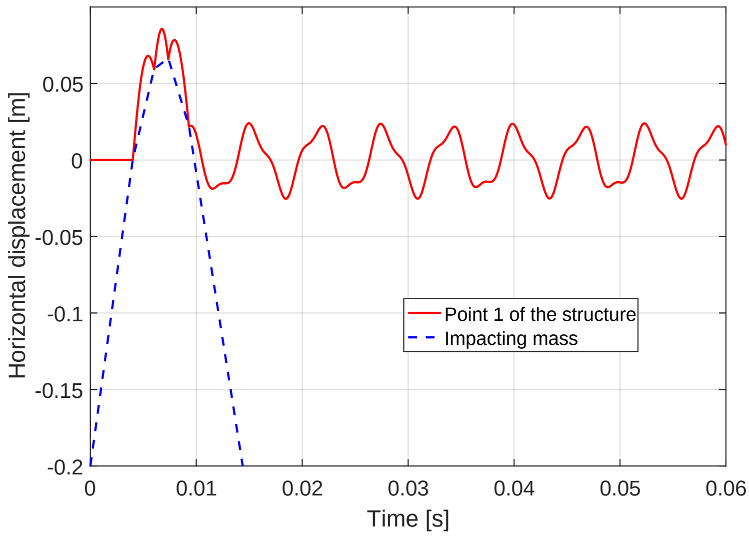

(a) Evolution of horizontal displacements

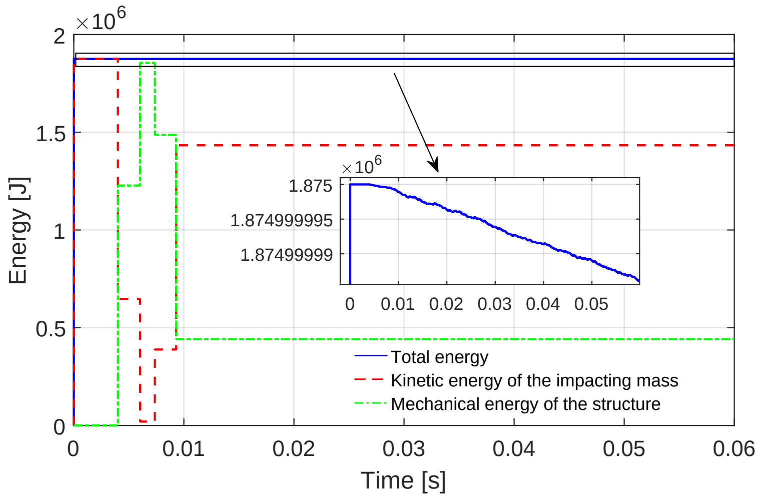

(b) Evolution of energies

Figure 6: Example 1: Elastic response with $\varepsilon = 1$

In order to show the conservation of energy in the case of elastic behaviour, this example is now run by considering elastic material and the restitution coefficient $\varepsilon = 1$. The results, depicted in Figs. 6(a) and 6(b), show that the total energy of the system is conserved during and after the contact.

6.2. *Example 2*

This example presents a steel frame structure with five spans and two storeys, the dimension of which is illustrated in Fig. 7(a). The structure is impacted at the middle column by a rigid point

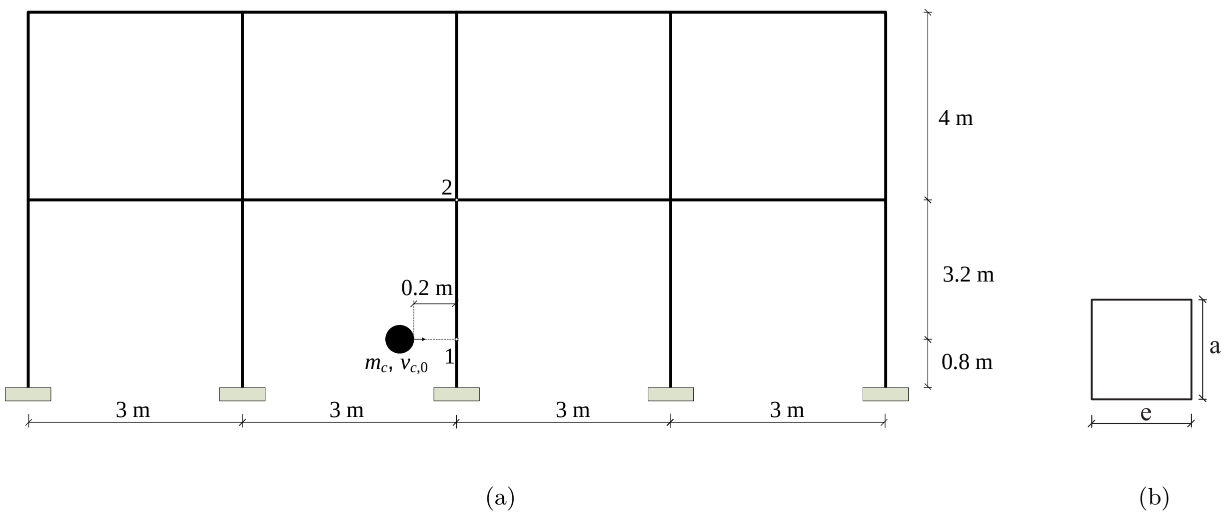

Figure 7: Example 2: (a) geometry. (b) cross-section.

mass $m_c = 1500\,\mathrm{kg}$ with an initial velocity of $v_{c,0} = 50\,\mathrm{m/s}$. The rest of the parameters are kept the same as Example 1.

For this example, 19 elements are used: one element for one member except for the impacted column that requires two elements. For the FE simulation, 1280 elements (element size $= 50\,\mathrm{mm}$) are needed to obtain a converged solution.

Fig. 8(a) and 8(b) show the evolution of the displacement of point 1 in the horizontal direction and of point 2 in the vertical direction, respectively. As can be seen from both figures, the proposed formulation gives results that are in good agreement with the reference solution. From Fig. 8(a), the difference in the maximum displacement of point 1 in horizontal direction between the proposed formulation and the reference FE simulation is around 0.5 percent. From Fig. 8(b), the difference in the maximum displacement of point 2 in vertical direction between the proposed formulation and the reference FE simulation is about 8.5 percent. It can also be observed that the same results are obtained with linear and nonlinear inertial expressions.

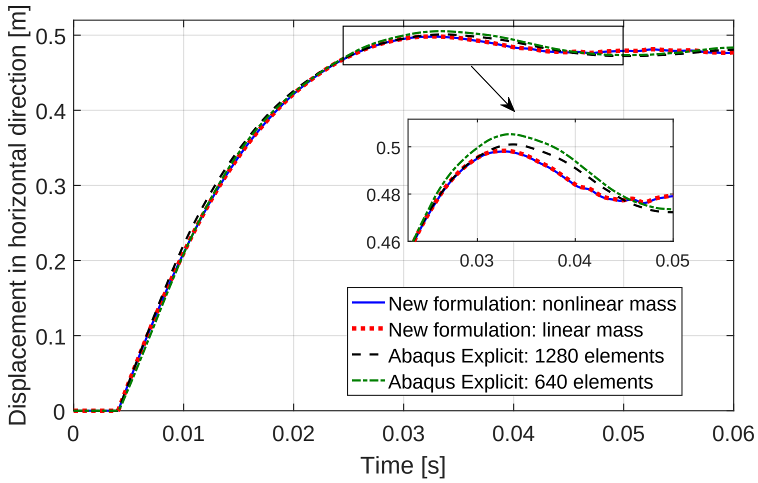

(a) Point 1

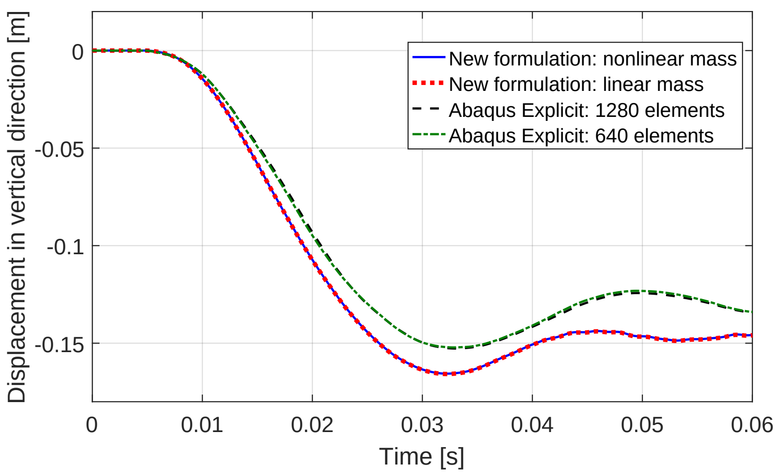

(b) Point 2

Figure 8: Example 2: Evolution of displacement

6.3. Example 3

The purpose of this example is to show the ability of the proposed formulation in capturing the main features of the inelastic behaviour of the steel frame structure and its connections under impact loading. This example considers a steel frame structure with five beam spans and two storeys, as depicted in Fig. 9. The cross-section types of the columns and of the beams are HEB 240 and IPE 240, respectively. The structure is impacted at the middle column by a rigid point mass $m_c = 1500\,\mathrm{kg}$ with an initial velocity of $v_{c,0} = 20\,\mathrm{m/s}$. The properties of the cross-section of

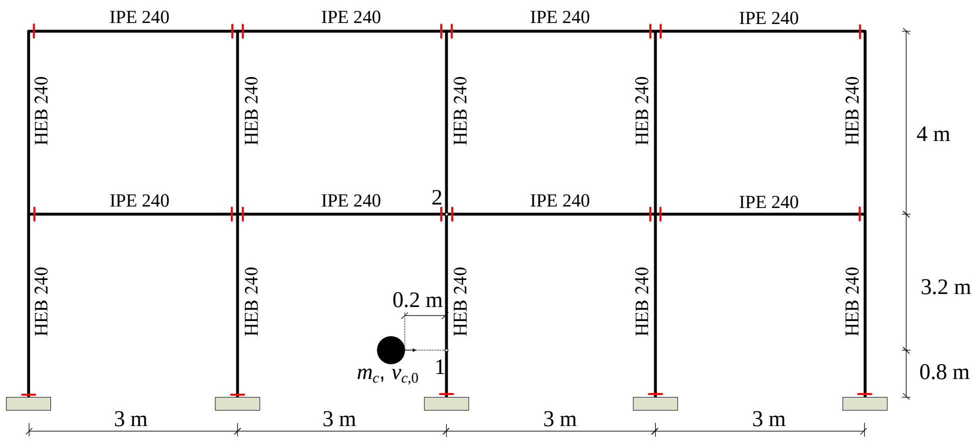

Figure 9: Example 3: geometry and location of joint

the structure members are defined in Table 1.

The configuration of the beam-to-column joint is illustrated in Fig. 10(a). The IPE-240 beam is welded to an end plate with dimensions of 364 mm × 160 mm × 15 mm, and the end plate is connected to the column's flange by eight 10.9 graded M20 bolts. The yield strength and the Young modulus of the components in the joint are 355 MPa and 210 000 MPa, respectively.

To assess the properties of the joint, the component method proposed in Eurocode 3 [22] is adopted. The component method corresponds to the simplified mechanical model that is composed of extensional springs and rigid links. More precisely, the mechanical model, described in Fig. 10(b), is composed of a column web's center line (first rigid link) connected to the beam end (second rigid link) by a number of effective springs. Working only in tension, spring T_1 combines the stiffness of the column's web in tension action, the column's flange in bending action and a bolt in tension action. Like spring T_1 that works only in tension, spring T_3 combines the stiffness of the column's web in tension action, the column's flange in bending action, the beam's web in tension and a bolt in tension. On the other hand, the spring T_2 works only in compression and corresponds to the combined effect of the column's web in compression, the beam's web and flange in compression and the column's web panel in shear. The rotational stiffness of the joint is determined according to Eurocode 3 [22], and the obtained value is $k_{\bar{\theta},j} = 1.2 \times 10^7$ Nm/rad with the stiffness ratio $\mu = 2$. Since Eurocode 3 does not mention any method to determine the axial stiffness of the joint, we decide to choose the axial stiffness of the joint by considering that the joint is under pure compression. The value of the axial stiffness obtained is $k_{\bar{u},j} = 1.5 \times 10^9$ N/m.

Table 1: Properties of the cross-section of the structure members

Type	Symbol	Beam IPE 240	Column HEB 240
Young modulus [MPa]	E	210 000	
Yield strength [MPa]	σ_y	355	
Nominal weight [GPa]	m_l	30.7	83.2
Section area [cm^2]	A	39.1	106
Second moment of area [cm^4]	I	3892	11260
Axial resistance [N]	N^p	1388050	3763000
Bending resistance [Nm]	M^p	130285	373815
Yield function	$\Phi = \left\lvert \frac{M}{M^p} \right\rvert + \left\lvert \frac{N}{N^p} \right\rvert^{1.3} - 1$		

Furthermore, the M-N interaction curve of the beam-to-column joint is determined by the method proposed by Cerfontaine [23]. The result is given in Fig. 11. This nonlinear M-N interaction is approximated by the authors in this paper using a linear M-N interaction.

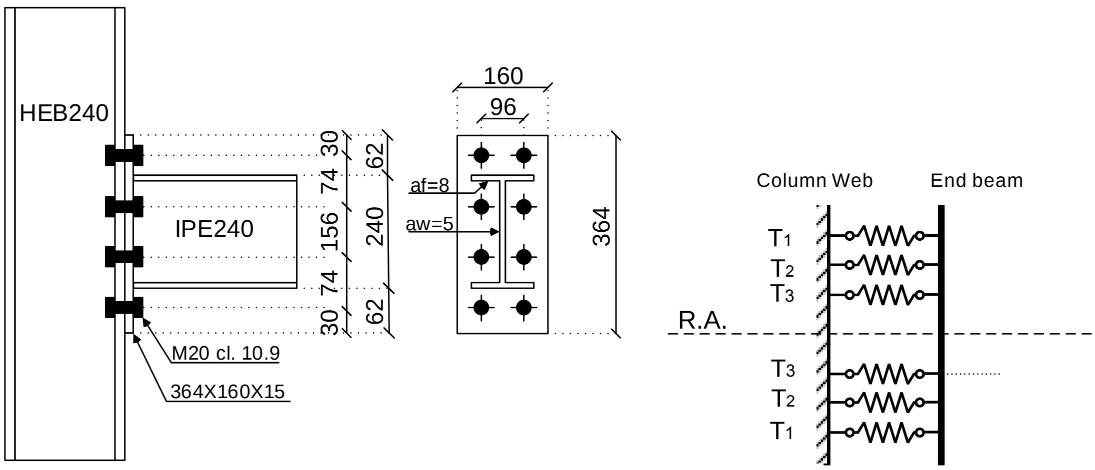

(a) (b)

Figure 10: (a) Configuration of the beam-to-column joint. (b) Mechanical model

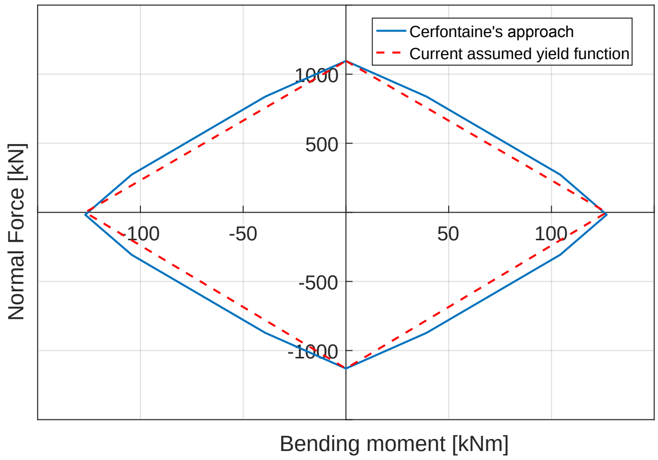

Figure 11: M-N interaction of the beam-to-column joint

The configuration of the column base joint is shown in Fig. 12 where the properties and dimensions of each component are given. In this joint, the column is welded to a base plate with the dimension of $470\text{mm} \times 330\text{mm} \times 25\text{mm}$ that is bolted to the foundation concrete block by eight embedded M24 anchor bolts with a steel grade of 10.9. The concrete type used for the concrete block is C30/37. The same concept of the mechanical model is also applied to the column base joint to find both the stiffness and the M-N interaction of the joint. The M-N interaction curve of the column base joint is presented in Fig. 13. With the same procedure as the beam-to-column joint, the axial and rotational stiffness of the column base are obtained as $k_{\bar{u},j} = 1.8 \times 10^9 \text{N/m}$ and $k_{\bar{\theta},j} = 0.84 \times 10^7$ Nm/rad, respectively. Two cases are studied. In the first one, without joints, rigid connections between the beams and the columns as well as between the column bases and the ground are assumed. In the second one, with joints, semi-rigid connections as defined in Figs. 10 and 12 are considered.

The evolutions of the horizontal displacement of point 1 and the vertical displacement of point 2 are depicted in Figs. 14(a) and 14(b), respectively. Significant differences between the two studied cases can be observed. This example shows that the response of the structure is considerably influenced by the inelastic behaviour of the joints and that the proposed formulation can include the effect of the semi-rigid joints.

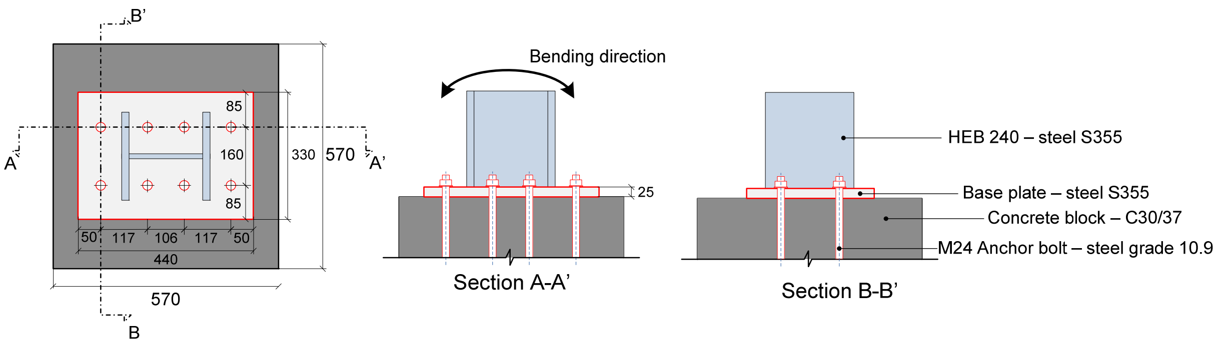

Figure 12: Configuration of column base joint

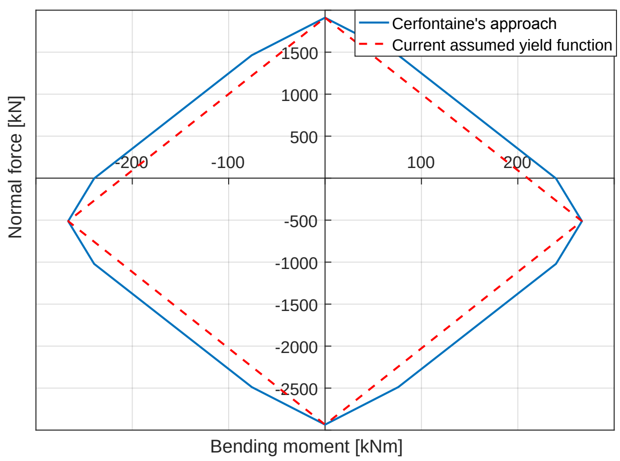

Figure 13: M-N interaction of the column-base joint

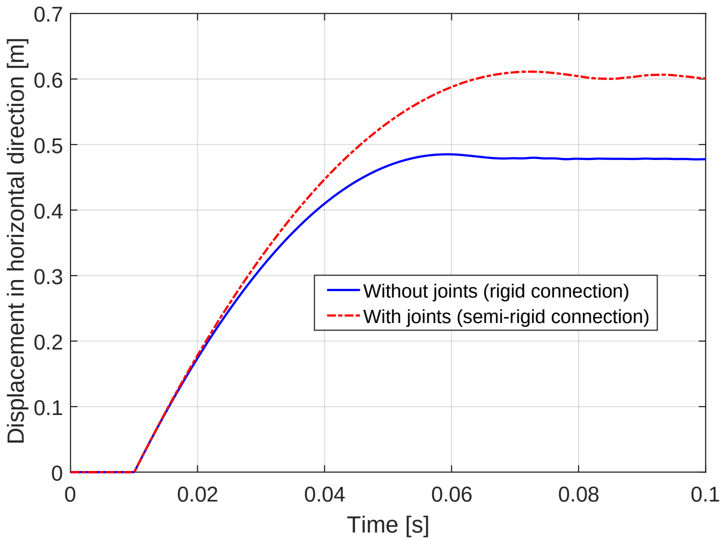

(a) Point 1

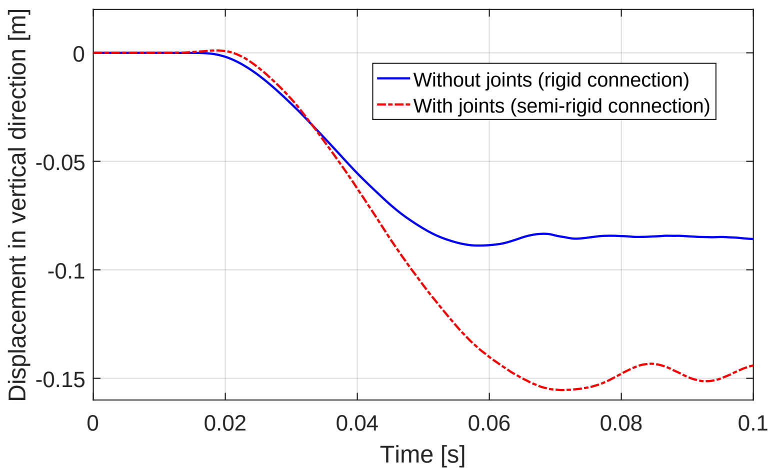

(b) Point 2

Figure 14: Example 3: Evolution of displacement

7. Conclusion

In the this paper, a 2D rigid beam element with generalized elasto-plastic hinges has been presented. The purpose of the formulation is to analyse the inelastic dynamical behaviour of steel frame buildings subjected to impact loading. The main features of the current model are the following. Firstly, the model is simple, efficient and accurate. The model is well integrated into the co-rotational framework and is able to accurately reproduce the geometrically nonlinear inelastic behaviour of the steel frame structures with a considerably smaller number of elements compared to the plastic zone approach. Secondly, the present model has the ability to capture the inelastic behaviour of the semi-rigid connections by the means of the generalized elasto-plastic hinges that are governed by the so-called superelliptic yield surfaces. Third, the equations of motion are written and solved using a consistent energy and momentum conserving scheme. Finally, the nonsmooth dynamics of the impact is treated in a rigorous framework, in which the equations of motion are derived using a set of differential measures and with the help of convex analysis tools. The velocity jump is described by the Newton's impact law using a restitution coefficient to accommodate possible energy losses at the contact. The present formulation could be potentially extended to 3D beams without any major difficulty.

Acknowledgements

The authors gratefully acknowledge financial support by the European Commission (Research Fund for Coal and Steel) through the project ROBUST-IMPACT under grant agreement RFSR-CT-2012-00029.

References

References

[1] Jean-Marc Battini, Costin Pacoste, Plastic instability of beam structures using co-rotational elements, Computer Methods in Applied Mechanics and Engineering, Volume 191, Issues 51–52, 20 December 2002, Pages 5811-5831, ISSN 0045-7825.

[2] Alsafadie, R., Battini, J.-M., Hjiaj. M., , Efficient local formulation for elasto-plastic corotational thin-walled beams, Communications in Numerical Methods in Engineering, International Journal for Numerical Methods in Biomedical Engineering, 27(4), (2011): 498-509.

[3] Foley, C.M., Vinnakota, S., Inelastic behavior of multistory partially restrained steel frames. Part I, J Struct Eng—ASCE 1999;125:862–9.

[4] Kim, S.-E, Lee, D. H., Second-order distributed plasticity analysis of space steel frames, Engineering Structures, Volume 24, Issue 6, June 2002, Pages 735-744, ISSN 0141-0296, http://doi.org/10.1016/S0141-0296(01)00136-5. (http://www.sciencedirect.com/science/article/pii/S0141029601001365)

[5] Sansour, C., Nguyen, T. L., Hjiaj, M., Energy-momentum method for in-plane geometrically exact Euler-Bernoulli beam dynamics. International Journal for Numerical Methods in Engineering 2015 102 (2):99–134.

[6] Liew, J., Chen, H., Explosion and Fire Analysis of Steel Frames Using Fiber Element Approach. J. Struct. Eng., 10.1061/(ASCE)0733-9445(2004)130:7(991), 991-1000.

[7] Nguyen, P.-C., Doan, N. T. N., Ngo-Huu, C., Kim, S.-E., Nonlinear inelastic response history analysis of steel frame structures using plastic-zone method, Thin-Walled Structures, Volume 85, December 2014, Pages 220-233, ISSN 0263-8231, http://doi.org/10.1016/j.tws.2014.09.002.

[8] Attalla, M., Deierlein, G., McGuire, W., Spread of Plasticity: Quasi-Plastic-Hinge Approach, Journal of Structural Engineering 120, no. 8 (August 1, 1994): 2451–73. doi:10.1061/(ASCE)0733-9445(1994)120:8(2451).

[9] Ngo-Huu, C., Kim, S.-E., Oh, J.-R., Nonlinear analysis of space steel frames using fiber plastic hinge concept. Engineering Structures, Volume 29, Issue 4, April 2007, Pages 649-657, ISSN 0141-0296, http://doi.org/10.1016/j.engstruct.2006.06.008. (http://www.sciencedirect.com/science/article/pii/S0141029606002549)

[10] Ziemian, R., McGuire, W., Modified Tangent Modulus Approach, A Contribution to Plastic Hinge Analysis. J. Struct. Eng., 10.1061/(ASCE)0733-9445(2002)128:10(1301), 1301-1307.

[11] Liew, J., White, D., Chen, W., Second-Order Refined Plastic-Hinge Analysis for Frame Design. Part I. J. Struct. Eng., 10.1061/(ASCE)0733-9445(1993)119:11(3196), 3196-3216.

[12] Heng, P., Hjiaj, M., Battini, J.-M., A simplified model for nonlinear dynamic analysis of steel column subjected to impact. International Journal of Non-Linear Mechanics, Volume 86, November 2016, Pages 37-54, ISSN 0020-7462, http://dx.doi.org/10.1016/j.ijnonlinmec.2016.07.005.

[13] Crisfield, M.A., Shi, J., A co-rotational element/time-integration strategy for non-linear dynamics, International Journal for Numerical Methods in Engineering 37 (1994) 1897–1913.

[14] Pacoste, C. Eriksson, A., Beam elements in instability problems, Computer Methods in Applied Mechanics and Engineering 144 (1997) 163–197.

[15] Battini, J.-M., Pacoste, C., Co-rotational beam elements with warping effects in instability problems, Computer Methods in Applied Mechanics and Engineering 191 (2002) 1755–1789.

[16] Le, T.-N., Battini, J.-M., Hjiaj, M., Efficient formulation for dynamics of corotational 2D beams, Computational Mechanics 48 (2011) 153–161.

[17] Chhang, S., Sansour, C., Hjiaj, M., Battini, J.-M., An energy-momentum co-rotational formulation for nonlinear dynamics of planar beams, Computers & Structures, Volume 187, 15 July 2017, Pages 50-63, ISSN 0045-7949, http://doi.org/10.1016/j.compstruc.2017.03.021.

[18] Xu, J., Lee, C.K., Tan, K.H. A two-dimensional co-rotational Timoshenko beam element with XFEM formulation, Comput Mech (2012) 49: 667. doi:10.1007/s00466-011-0670-x

[19] Doan, N. T. N., Dang, X.-L., Chu, Q.-T., Balling, R.J., Ngo-Huu, C., Second-order plastic-hinge analysis of planar steel frames using corotational beam-column element, Journal of Constructional Steel Research, Volume 121, June 2016, Pages 413-426, ISSN 0143-974X, http://doi.org/10.1016/j.jcsr.2016.03.016.

[20] Alhasawi, A., Heng, P., Hjiaj, M., Guezouli, S., Battini, J.-M., Co-rotational planar beam element with generalized elasto-plastic hinges. Engineering Structures 158, (2017): 188-205.

[21] Moreau, J.J., Unilateral Contact and Dry Friction in Finite Freedom Dynamics. in Non-smooth Mechanics and Application, CISM Courses and Lectures, J.J. Moreau and P.D. Panagiotopoulos, Editors. 1988, Springer: Wien. p. 1-82.

[22] EN 1993-1-8, Eurocode 3: Design of steel structures, part 1.8: design of joints. Brussels: European Committee for standardization; 2005.

[23] Cerfontaine, F, Etude analytique de l'interaction entre moment de flexion et effort normal dans les assemblages boulonnés. Construction métallique 38, no. 4 (2001): 3-30.